Plasmon spectroscopy: Robust metallicity of Au wires on Si(557) upon oxidation

Z. Mamiyev,[1,2] T. Lichtenstein,[1] C. Tegenkamp,[1,2] C. Braun,[3] W. G. Schmidt,[3] S. Sanna,[4,*] and H. Pfnür[1,2,†]

[1]*Institut für Festkörperphysik, Leibniz Universität Hannover, Appelstraße 2, 30167 Hannover, Germany*

[2]*Laboratorium für Nano- und Quantenengineering (LNQE), Leibniz Universität Hannover, Schneiderberg 39, 30167 Hannover, Germany*

[3]*Lehrstuhl für Theoretische Materialphysik, Universität Paderborn, 33095 Paderborn, Germany*

[4]*Institut für Theoretische Physik, Justus-Liebig-Universität Gießen, Heinrich-Buff-Weg 16, D-35392 Gießen, Germany*

(Received 20 April 2018; revised manuscript received 31 May 2018; published 15 June 2018)

We investigated initial steps of oxidation of the Si(557)-Au system by plasmon spectroscopy and first-principles calculations. The measurements, performed using an electron energy loss instrument with simultaneous high resolution in energy and momentum, reveal that metallicity is preserved under all oxidation conditions that are experimentally accessible in UHV. Corresponding simulations, performed within density functional theory, confirm this finding: Only the oxidation of the Si environment of the Au chains turned out to be strongly exothermic, with similar binding energy for adsorption on different structural elements. While large and site specific changes of the band structure were observed, the upper edge of the excitation spectrum of electron-hole pairs, to which plasmon dispersion is most sensitive, remains almost unchanged during the various steps of oxidation, due to the opposite and largely compensating contributions of different adsorption configurations. This investigation not only proves the robustness of metallicity of the gold chains upon oxidation of the surrounding environment of Si atoms, but also demonstrates the usefulness of plasmon spectroscopy in characterizing the electronic excitation spectrum of quasi-one-dimensional systems and unoccupied band structure.

DOI: 10.1103/PhysRevMaterials.2.066002

I. INTRODUCTION

Quasi-one-dimensional (1D) electronic systems have attracted a great deal of interest due to highly unusual properties such as quantization of conductance, extremes of electronic correlation manifested by spin-charge separation, charge and spin density waves [1,2], triplet superconductivity, and Luttinger liquid behavior [3–5]. Due to their inherent instability, however, structural embedding and understanding of the coupling to other dimensions is of high relevance and raises the question of how much of 1D properties survives under experimentally accessible conditions. Fortunately, many 1D properties can still be observed in these quasi-1D systems [6–10].

The close relationship between low-energy plasmons and metallicity is well established in all dimensions [11]. Particularly in two and one dimensions, the plasmonic dispersion goes to zero in the long wavelength limit [12]. In this limit, a linear dispersion for plasmons in quasi-1D metallic wires is predicted [13]. Atomic wires thus are ideal candidates for directed energy transport on the nanoscale. Such dispersions have indeed been found for regular arrays of atomic wires on insulating substrates [14–16]. Moreover, confinement effects in these metallic subunits on the surface lead to the formation of intersubband excitations [15–18].

The vicinal Si(111) surfaces represent an interesting playground in this context, since either single or double Au chains are formed on these surfaces, depending on the step orientation. While, e.g., on Si(553) and Si(775), double chains are observed [8,19–22], the (335) and (557)-oriented Si-Au systems form wires with only a single atomic Au chain on each terrace [19,23]. The origin of this remarkable difference can only be due to the different type of step edge, which (formally) exhibits two dangling bonds per step edge atom compared to only one on the Si(553)-Au and Si(775)-Au surfaces. Common to all these structures is a Si-honeycomb chain located at the step edges [8,19,20]. While plasmon dispersions in such systems turned out to be purely 1D [24–26], a clear dependence of slopes on terrace widths and structural motif of the gold chains was found, taken as indications of dimensional crossover, as well as plasmonic coupling between the wires in the ordered arrays [26–29].

In this paper we extend previous studies of such systems [16,26,29,30] and test the robustness specifically of the Si(557)-Au system, containing a single atomic chain per terrace, against oxidation of its environment. This study has some relevance since oxidation is the first modification that will take place when such samples are brought into the environment.

As a further purpose of the present study, we extend our tests of the predictions of quasi-1D plasmon theory [25,28] and in particular the close relationship between the plasmon dispersion and the continuum of electron-hole pair excitations characteristic for a metallic system, which we started very recently [29]. We demonstrated that the comparison of this continuum, as derived from band structure calculations, with experimental data of plasmon dispersion can yield direct information about the form of the occupied as well as of the unoccupied band structure in the vicinity of the Fermi level [29]. Using different Si(111) vicinal surfaces as test systems, and combining experimental electron energy loss spectroscopy with quantitative density-functional theory (DFT) calculations,

*Simone.Sanna@theo.physik.uni-giessen.de

†pfnuer@fkp.uni-hannover.de

we illustrated this relationship between electronic band structure and plasmon dispersion.

In this paper we employ a similar approach to explore the possibility of tuning the electronic conductivity by post-adsorption of oxygen atoms on Si(557)-Au. In particular, we combine plasmon spectroscopy and DFT to investigate the effects of oxidation on this system. Since metallicity turns out to be quite robust under this treatment, our investigation may be considered as an important step towards the embedment of quasi-1D structures, in which the new environment might be used to finely manipulate the properties of the conducting structure.

II. METHODOLOGY

A. Experimental setup

All experiments were performed in an ultrahigh vacuum chamber operating at a base pressure of 5×10^{-11} mbar. It hosts a high resolution spot profile analysis low energy electron diffractometer (SPA-LEED) to investigate and control the sample quality, and a combination of an electron energy loss spectrometer with a LEED diffractometer (EELS-LEED) providing high resolution both in energy and momentum [31] in order to determine plasmon dispersion relations. The Si(557) sample ($\rho \approx 0.01\ \Omega$cm, n type) was degassed at 600 °C overnight followed by annealing to 1250 °C for a few seconds and then rapid cooling to room temperature. The overall sample quality was checked by SPA-LEED.

The Au coverage was evaporated from a gold pearl located on a tungsten filament by putting direct current through the filament at a substrate temperature of 630 °C. The coverage was controlled and calibrated by quartz microbalances placed at the position of the samples [32]. After Au deposition and cooling to room temperature the samples were quickly annealed to 930 °C for <1 s, followed by instantaneous cooling to room temperature. The loss measurements were carried out directly after this post-annealing step in order to avoid any influence of residual gas on surface and electronic structure. For adsorption measurements O_2 was dosed to the sample by an increase of background pressure to $\approx 2 \times 10^{-8}$ mbar via a separate gas line. After a certain exposure the oxygen flow was stopped and when the pressure dropped below 2×10^{-10} mbar EEL spectra were recorded.

In order to make the data comparable, in particular the loss peak positions, identical fitting routines were used for the EEL spectra. They fit the elastic peak with Gaussians, the Drude tail with an exponential energy dependence, while loss peaks were fitted by exponentially modified Gaussians in order to account for their asymmetry. Details are described in Ref. [30].

B. Calculations

Au nanowires on the Si(557) surface were modeled within the density functional theory, as implemented in the Vienna *ab initio* simulation package (VASP) [33,34]. Thereby we performed total-energy calculations within the generalized gradient approximation (GGA) in the Perdew-Burke-Ernzerhof (PBE) formulation [35,36]. Projector augmented wave (PAW) potentials [37,38] with projectors up to $l = 1$ for H, $l = 2$ for Si and O, and $l = 3$ for Au. A number of 1 ($1s^1$), 4 ($3s^2 3p^2$), 6 ($2s^2 2p^4$), and 11 ($5d^{10} 6s^1$) valence electrons were employed for the simulation of H, Si, O, and Au atoms, respectively. The electronic wave functions were expanded into plane waves up to an energy cutoff of 410 eV. A $4 \times 12 \times 1$ Monkhorst-Pack [39] k-point mesh was used to perform the integration in the Brillouin zone. The Si(557)-Au system was modeled by a (5×2) slab containing 2 Au and a total of 147 atoms. The asymmetric slab consisted of six Si bilayers stacked along the [111] crystallographic direction modeling the substrate, the surface termination including the Au chain, and a vacuum region of about 20 Å. Hydrogen atoms saturate the dangling bonds at the lower face of the slabs. A dipole correction [40,41] was used to quench the electric field between the slab and its periodic images. The atomic positions were relaxed until the residual Hellmann-Feynman forces were lower than 0.01 eV/Å. Three Si bilayers and the hydrogen atoms were kept constrained in order to model the substrate, while the silicide film and three Si bilayers were free to relax. Oxygen adsorption sites and geometries correspond to the stable adsorption configurations first determined in Ref. [42].

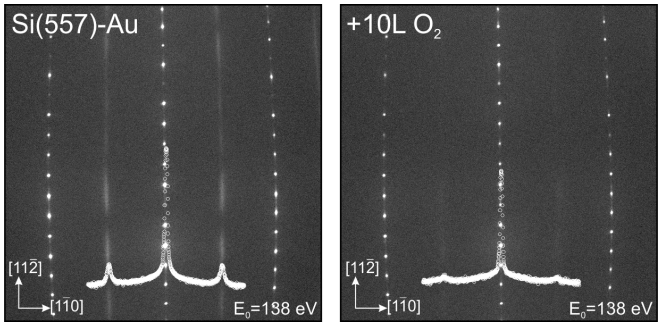

FIG. 1. SPA-LEED patterns of Si(557)-Au surface before (left) and after (right) adsorption of 15 L of oxygen (1 L = 1×10^{-6} mbar s): The overlayer curves depict the 1D-line scans along the [1$\bar{1}$0] direction.

III. RESULTS

The adsorption of 0.19 monolayers (ML) of Au generated a LEED pattern characteristic of a regularly and doubly stepped Si(557) surface with considerably improved order compared to the clean surface and sharp ×2 streaks that are generated mainly by pairing of the Si atoms in the adatom row [43,44]. The resulting LEED patterns after surface preparation and upon oxidation are given in Fig. 1. The spot splitting of 18% of the surface Brillouin zone (SBZ) corresponds to a periodicity of $5\frac{2}{3} a_\perp / \cos 9.5°$ ($a_\perp = 3.32$ Å is the substrate lattice vector along the [11$\bar{2}$] direction) that is in good agreement with previous studies [24,42].

This structure shows clear plasmonic losses whose dispersion is in good agreement with previously published results [24,25,29]. A set of sample spectra is shown in the left part of Fig. 2. The nearly exponential decay of the structureless background at low $k_\parallel$, known as Drude tail, is a clear indication of metallicity, i.e., of the low-energy continuum excitations within the conduction band(s). Peak positions of plasmon losses were determined using a fitting routine including subtraction of the Drude tail, as described in detail in Ref. [30].

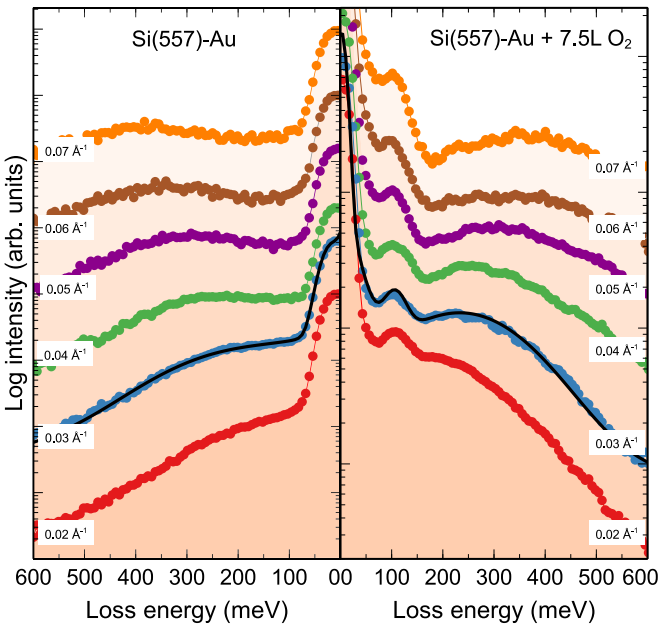

FIG. 2. EEL spectra of the Si(557)-Au system for k vectors parallel to wire direction. Left-hand side: Clean surfaces. Right-hand side: After adsorption of 7.5 L of O_2. In both cases, a dispersing loss is only seen in the $[1\bar{1}0]$ direction parallel to the steps. The black lines in the second spectra from bottom are fits according to the procedure described in Ref. [30].

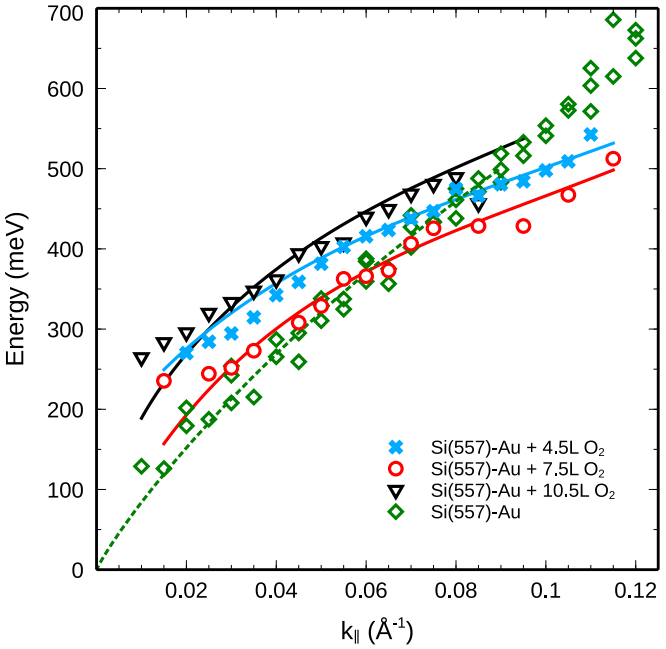

FIG. 3. Plasmon dispersion of the clean Si(557)-Au system (⋄) and after various doses of oxygen, as indicated. The green dashed line corresponds to the fit of Ref. [25] with harmonic confinement (width 4 Å) of a 2D nearly free electron gas. Solid lines are guides to the eye with the assumption that the curves have to start at $E = 0$ in the long wavelength limit.

Surface conductance measurements showed that conductance in the direction along the wires decreases by about 20% within the first 10 Langmuir (1 L $= 1 \times 10^{-6}$ mbar s) of oxygen exposure [42], followed by a slow further decrease of additional 10% up to an exposure of 35 L. Thus metallicity is not lost by oxygen exposure, but we expected to also see a clear decrease of the plasmon loss energy upon exposure to oxygen. Oxygen adsorption at room temperature, however, turned out to partly even increase the plasmon loss energy. The spontaneous dissociation of oxygen is clearly evident from the appearing loss peak at 110 meV, which is due to the formation of Si-O bonds and their vibrational excitation. This loss appears shifted to smaller energy on the stepped and Au-covered surface compared with flat Si(111) [45]. Although the increasing oxygen exposure introduces disorder into the surface layer, as evident from the decreasing intensity and final disappearance of the $\times 2$ streaks in LEED (see Fig. 1), the plasmonic loss seems to be almost unaffected, as we will discuss in the following.

These results are summarized in the measured dispersion curves shown in Fig. 3. Compared to the pristine Si(557)-Au system, the curves obtained after various doses of oxygen are less dispersive, so that the data points after oxygen exposure are below those of the pure system at high $k_\parallel$ and above them at low $k_\parallel$. Furthermore, the nonmonotonic shift of the dispersion curves as a function of oxygen exposure is remarkable and needs to be explained.

We start with the low-k behavior. While this overall change of slope can only be caused by significant changes in the band structure (as revealed by the DFT calculations shown below), oxygen dissociation and adsorption also introduces an increasing degree of disorder into the system. Thus, scattering probabilities of plasmonic waves are increased up to the limit of total reflection and the formation of standing waves. As a consequence, deviations from the "ideal" curve, particularly at low k, are expected, leading to finite plasmon loss energies in the limit of $k_\parallel \to 0$. These properties are nicely demonstrated here. Almost ideal behavior is indeed seen for the pure Si(557)-Au system, in which dispersion goes to zero in the long wavelength limit within experimental uncertainties (green dashed line in Fig. 3). For the oxygen covered surface, however, extrapolations of the data to $k = 0$ always end at finite energies. In order to visualize the deviations from the system without disorder, we inserted schematically the solid lines through the data points at various stages of oxidation assuming that the curves have to start at the origin.

For a more quantitative analysis of the plasmon dispersion, we refer to the approach used in Ref. [29], using the fact that there is a close relationship between the upper edge of the electron-hole continuum and the plasmon dispersion, which for quasi-1D systems turns out to be particularly simple. If the quasi-1D array of wires is considered as a 2D electron gas that is confined to a wire of finite width by an appropriate potential [25], the plasmon dispersion for a single isolated wire can be expressed as a function of the upper and lower boundary of the electron-hole continuum of excitations ω_+ and ω_-, respectively, as follows:

$$\omega_p(k_\parallel) = \sqrt{\frac{\omega_+^2(k_\parallel)e^{A(k_\parallel)} - \omega_-^2(k_\parallel)}{e^{A(k_\parallel)} - 1}} \qquad (1)$$

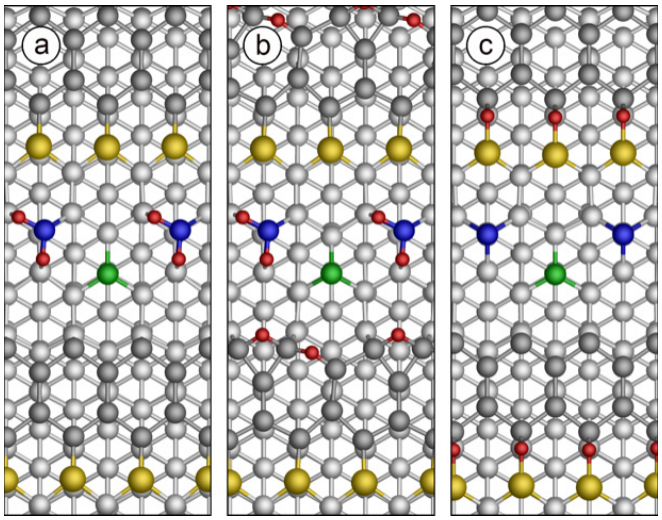

FIG. 4. Geometrical models of the oxidized Si(557)-Au system. (a)–(c) Oxygen adsorbed at the Si-adatom, adatom and honeycomb chain, and between honeycomb and Au chain, respectively. Yellow: gold chain, gray: topmost Si atom layer, dark gray: Si honeycomb chain (upper edge corresponds to step edge), blue: Si adatom row, green: Si rest atom row, red: oxygen atoms.

with

$$A(k) = \frac{\hbar^2 2\pi k}{m^\star g_s V(k)[1 - G(k)]}.$$

$V(k)$ is the Fourier transform of the confining potential, $G(k)$ is the local field correction factor due to electronic correlations, and g_s is the spin degeneracy (1 or 2). This formula, which is not limited to a nearly free electron gas, shows the intimate relationship between the continuum of e-h excitations and the plasmon dispersion. By solving Eq. (1) with respect to ω_+, using the experimentally determined plasmon dispersion and ω_- (from the calculated band structures) as inputs, ω_+ can now be directly compared with the excitation spectrum of a calculated band structure. As we will show, Eq. (1) sets important boundaries to the validity of certain models.

In order to get an idea of the modifications of the band structure by dissociative oxygen adsorption, band structures for the stable adsorption geometries determined in Ref. [42] have been calculated. The DFT models reveal that O adsorption directly at the Au sites is unfavorable, whereas Si-adatom and the Si-HC sites are strongly preferred (see Fig. 4 for details) with binding energies up to 8 eV. This site-specific adsorption behavior for oxygen already explains the changes of the LEED patterns and disappearance of the $\times 2$ diffraction spots upon adsorption, since it lifts the adatom periodicity. There are several sites with comparable binding energies. Thus, kinetics is expected to play an important role in their occupation. This statement remains valid for higher average concentrations of oxygen, as tested, e.g., by comparing oxidation of HC sites after complete oxidation of the adatom row.

The band structures of the Si(557)-Au after oxidation of the various structural motifs of Fig. 4 are shown in Fig. 5 in an extended zone scheme, with a restriction to those bands with clear contributions from the Au chain, adatoms, and the HC chain. In Fig. 5(a) the complete adatom row has been

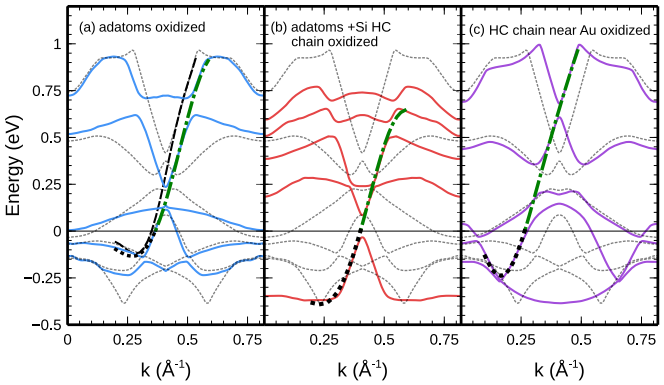

FIG. 5. Band structures calculated in an extended zone scheme along $\overline{\Gamma Y}$ ($\bar{Y}$ at 0.82 Å^{-1}) according to the structural models represented in Figs. 4(a)–4(c), respectively. The black dashed lines below the Fermi level (E_F, energy zero) correspond to the assumed $\hbar\omega_-$. Above E_F $\hbar\omega_+$ is plotted (dashed-dotted line, green) which was calculated from the experimental plasmon dispersion and $\hbar\omega_-$ according to Eq. (1), as described in the text. The black dashed line in (a) indicates the analogous result for the clean system.

oxidized. As expected, modifications of the bands associated with the adatoms and the restatoms were observed due to the admixture of oxygen orbitals, but changes to the band with preferential Au character are surprisingly small, as obvious by the comparison with the bands of the pure Si(557)-Au system, which are shown as thin dotted lines in this figure. A single band crosses the Fermi level, and the Fermi wave vector slightly changes from 0.35 Å to $k_F = 0.37$ Å. These changes get stronger with increasing oxygen concentration, as seen in Fig. 5(b). Although the configuration of Fig. 4(c) is energetically not very favorable, i.e., these sites will only be filled after those shown in Figs. 4(a) and 4(b), it was used to test the effect of oxidation of Si atoms in the immediate vicinity of the Au chain. As seen in Fig. 5(c), even under these conditions the system remains metallic.

Turning now to the analysis of the plasmon dispersion and its relation to the boundaries of the e-h continuum, ω_+ and ω_-, the analysis is similar to the pure system [29] and unique, since only one band is crossing the Fermi level in each Brillouin zone. As already mentioned above, the lowest possible excitations from the occupied bands to the Fermi level, which corresponds to $\hbar\omega_-$, was determined from the calculated band structures shown in color in Fig. 5. In our case, $\hbar\omega_-$ is equivalent to the thick dashed line at *negative* energies, i.e., below the Fermi level. $\hbar\omega_+$ was now calculated using these values of $\hbar\omega_-$ together with the *experimental* dispersion $\hbar\omega_p$ obtained as the average values of the experimentally determined plasmon dispersion curve at each $k_\parallel$ point. Furthermore, for calculating $A(k)$ we assumed a Gaussian distribution of the electrons in the system with a FWHM of 3.3 Å, corresponding to a single atomic wire. This width corresponds to a parabolic confinement with ground state width of 1.4 Å or, approximately, to a square-well confinement of 6.6 Å. These parameters, together with an effective mass m^* at E_F, determine $A(k_\parallel)$. As tested, the results depend very little on the exact wire width. The effective mass close to E_F was determined by approximating the band for ω_- by a parabola near E_F. As an example, we

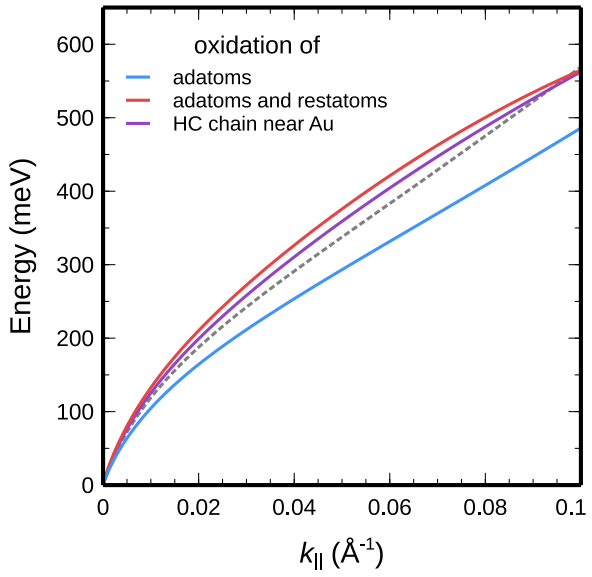

FIG. 6. Modifications of plasmon dispersion, as predicted from band structure calculations and the theory according to Eq. (1) after local adsorption of atomic oxygen at the various sites indicated in the legend. The dashed line represents the pristine Si(557)-Au surface.

got an effective mass of $m^* = 0.23\, m_e$, for the case of adatom oxidation shown in Fig. 5(a).

In fact $\hbar\omega_+$, indicated by the thick dashed lines above E_F in Fig. 5, closely coincides with $\hbar\omega_p$ (except near E_F) in all cases investigated. This line coincides nicely with the calculated band structure. As already seen for the pristine system [29], the small band gaps found in the calculations due to hybridization of the Au-induced band with the various structural elements of the Si surface, are integrated over in $\hbar\omega_+$, and the dashed line exhibits an almost linear dispersion, similar to the clean surface. Only the average slope in the quasilinear section above E_F is about 15% lower than in the pure system, as indicated by the thin dashed line in Fig. 5(a).

A more detailed comparison between clean and oxidized surfaces is shown in Fig. 6. For adatom oxidation it is marked as a blue line. The lower average slope at larger $k_{\|}$ reflects the lowering mainly of ω_+, as just discussed. We further note that there is also a change of curvature as already seen for the measured plasmon dispersion (see Fig. 3).

Similar procedures have been applied to the other models for oxidation of this system, i.e., oxidation of the HC chain near the Au chain [Fig. 5(c)] and the simultaneous oxidation of adatoms and the HC chain [Fig. 5(b)]. While the band structure exhibits significant changes, depending on the location of Si oxidation, there is also a varying net charge transfer, which results in up and down shifts of the Fermi level, seen as shifts of the whole band structures relative to the unoxidized band structure in Fig. 5. Nevertheless, the overall behavior of the upper edge of the excitation spectrum changes remarkably little, and is still determined by the metallicity of the Au channel. An exception in this respect is the opening of a small gap at E_F, when both adatoms and HC chains are oxidized. However, as already mentioned in Ref. [42], this gap opening is highly sensitive to the model geometries. Therefore, it is quite unclear to what extent such a gap opening will be relevant in experiment. The gap, indeed, may further be smeared out by disorder in the system.

The band structures of Figs. 5(b) and 5(c) have the opposite effect on the plasmon dispersion compared with the oxidation of the adatoms alone, as shown in Fig. 6. A tendency to increase plasmon frequency at low $k_{\|}$ is observed, yet the curves for the oxidized systems intersect that of the pure system at $k_{\|} = 0.1$ Å^{-1}.

Comparing these simulated results with the measured plasmon dispersions as a whole, we see that the nonmonotonic overall shift is qualitatively reproduced in the calculations, assuming that the Si HC chain first oxidize together with the adatoms, but with a preference of adatom oxidation, while further elements of the surface follow at a later stage. Due to the limitations of the atomistic models, the semiquantitative agreement between simulations and experiment can be considered as satisfactory. Due to the periodic boundary conditions, a complete and ordered array of oxygen adatoms is simulated. Our models thus neither take into account the mixture of adsorption sites that will necessarily happen in experiment nor the disorder introduced by (more or less) random adsorption. The simulations, however, describe nicely the observed robustness of metallicity in the system.

Our plasmon spectroscopy results complement measurements of dc conductance in this system [42]. A reduction of conductance as a function of oxygen dose and the transition from anisotropic to isotropic conductance was found, while total conductance was only reduced by about 20% within the range of oxygen exposure considered here. These results, which at first sight seem to partially contradict those presented here, mainly illustrate the complementarity of plasmon spectroscopy and dc conductance measurements for several reasons: Dc conductance mainly probes electronic states very close to the Fermi level, typically in the energy range of $k_B T$ set by the sample temperature, since electric fields are normally very weak. It is thus also very sensitive to changes in charge transfer and band filling close to E_F. Furthermore, charge carrier mobility enters directly dc conductance that is strongly influenced by disorder. Therefore, dc conductance is highly sensitive to disorder in the system. In addition, the contribution of space charge layers to the overall conductance cannot be excluded.

The situation is very different when plasmons are used to probe conductance. The unoccupied states accessible to plasmon spectroscopy experimentally are above 100 meV up to 1 eV. The position of plasmon losses is thus quite insensitive to small changes of the Fermi level, in contrast to dc conductance. Second, disorder changes plasmon frequencies only at small $k_{\|}$, which can be treated as a correction. Furthermore, the plasmons studied here are derived from surface states. Thus there cannot be any contribution from space charge layers. Both methods found that metallicity is altered in this system, but it is not destroyed by oxidation. The degree of measured changes, however, is specific to the method used.

IV. SUMMARY AND CONCLUSIONS

Using high resolution electron spectroscopy with high momentum resolution for detecting plasmons we show that in

Si(557)-Au, containing a single atomic gold chain per terrace, mainly the surrounding Si surface elements are oxidized by oxygen exposure at room temperature. This oxidation process modifies the metallic channel induced by the formation of the gold chain on the surface, but leaves metallicity intact on this surface, in agreement with transport measurements. This experimental finding is semiquantitatively supported by DFT calculations, which investigated the effect of oxidation of various structural motifs on the surface. Although calculations and experiment are not strictly comparable due to the assumption of ordered oxygen arrays adsorbed on specific sites, our approach allows us to describe a kinetic sequence of preferential adsorption. Thus plasmon spectroscopy turns out to be a valuable tool to get information about changes of the unoccupied part of the band structure—in this case induced by chemical reaction on the surface. Electrical surface transport measurements, on the other hand, detect detailed changes close to the Fermi level, to which plasmon spectroscopy has little sensitivity, underlining the complementarity of both experimental approaches.

ACKNOWLEDGMENTS

We gratefully acknowledge financial support from the Deutsche Forschungsgemeinschaft in the research unit FOR 1700 and Niedersächsisches Ministerium für Wissenschaft und Kultur through the graduate school "contacts in nanosystems." All the calculations were performed at the Paderborn Center for Parallel Computing (PC^2) and the High Performance Computing Center Stuttgart (HLRS).

[1] S. Kagoshima, H. Nagasawa, and T. Sambongi, *One Dimensional Conductors*, Springer Series in Solid-State Sciences (Springer, Berlin, 1988), Vol. 72, pp. 126–135.
[2] G. Grüner, Rev. Mod. Phys. **60**, 1129 (1988).
[3] J. M. Luttinger, J. Math. Phys. **4**, 1154 (1963).
[4] K. Schönhammer, *Strong Interactions in Low Dimensions*, Physics and Chemistry of Materials with Low-Dimensional Structures, edited by D. Baeriswyl and L. Degiorgi (Springer, Dordrecht, 2004), Vol. 25, Chap. 4, pp. 93–136.
[5] T. Giamarchi, *Quantum Physics in One Dimension* (Clarendon, Oxford, 2007).
[6] P. C. Snijders and H. H. Weitering, Rev. Mod. Phys. **82**, 307 (2010).
[7] H. Weitering, Nat. Phys. **7**, 744 (2011).
[8] S. C. Erwin and F. J. Himpsel, Nat. Commun. **1**, 58 (2010).
[9] J. Aulbach, J. Schäfer, S. C. Erwin, S. Meyer, C. Loho, J. Settelein, and R. Claessen, Phys. Rev. Lett. **111**, 137203 (2013).
[10] C. Brand, H. Pfnür, G. Landolt, S. Muff, J. H. Dil, T. Das, and C. Tegenkamp, Nat. Commun. **6**, 8118 (2015).
[11] A. Liebsch, *Electronic Excitations at Metal Surfaces* (Springer, Boston, 1997).
[12] J. M. Pitarke, V. M. Silkin, E. V. Chulkov, and P. M. Echenique, Rep. Prog. Phys. **70**, 1 (2007).
[13] S. Das Sarma and W.-y. Lai, Phys. Rev. B **32**, 1401 (1985).
[14] T. Nagao, S. Yaginuma, T. Inaoka, T. Sakurai, and D. Jeon, J. Phys. Soc. Jpn. **76**, 114714 (2007).
[15] E. P. Rugeramigabo, C. Tegenkamp, H. Pfnür, T. Inaoka, and T. Nagao, Phys. Rev. B **81**, 165407 (2010).
[16] U. Krieg, C. Brand, C. Tegenkamp, and H. Pfnür, J. Phys.: Condens. Matter **25**, 014013 (2013).
[17] T. Inaoka, Phys. Rev. B **71**, 115305 (2005).
[18] M. Smerieri, L. Vattuone, L. Savio, T. Langer, C. Tegenkamp, H. Pfnür, V. M. Silkin, and M. Rocca, Phys. Rev. Lett. **113**, 186804 (2014).
[19] J. N. Crain, J. L. McChesney, F. Zheng, M. C. Gallagher, P. C. Snijders, M. Bissen, C. Gundelach, S. C. Erwin, and F. J. Himpsel, Phys. Rev. B **69**, 125401 (2004).
[20] I. Barke, F. Zheng, T. K. Rügheimer, and F. J. Himpsel, Phys. Rev. Lett. **97**, 226405 (2006).
[21] J. Aulbach, S. C. Erwin, R. Claessen, and J. Schäfer, Nano Lett. **16**, 2698 (2016).
[22] M. Krawiec, Phys. Rev. B **81**, 115436 (2010).
[23] M. Krawiec and M. Jałochowski, Phys. Rev. B **87**, 075445 (2013).
[24] T. Nagao, S. Yaginuma, T. Inaoka, and T. Sakurai, Phys. Rev. Lett. **97**, 116802 (2006).
[25] R. K. Moudgil, V. Garg, and K. N. Pathak, J. Phys.: Condens. Matter **22**, 135003 (2010).
[26] T. Lichtenstein, J. Aulbach, J. Schäfer, R. Claessen, C. Tegenkamp, and H. Pfnür, Phys. Rev. B **93**, 161408 (2016).
[27] Q. Li and S. Das Sarma, Phys. Rev. B **41**, 10268 (1990).
[28] S. Das Sarma and E. H. Hwang, Phys. Rev. B **54**, 1936 (1996).
[29] T. Lichtenstein, Z. Mamiyev, C. Braun, S. Sanna, W. G. Schmidt, C. Tegenkamp, and H. Pfnür, Phys. Rev. B **97**, 165421 (2018).
[30] U. Krieg, T. Lichtenstein, C. Brand, C. Tegenkamp, and H. Pfnür, New J. Phys. **17**, 043062 (2015).
[31] H. Claus, A. Büssenschütt, and M. Henzler, Rev. Sci. Instrum. **63**, 2195 (1992).
[32] G. Sauerbrey, Z. Phys. **155**, 206 (1959).
[33] G. Kresse and J. Furthmüller, Comput. Mater. Sci. **6**, 15 (1996).
[34] G. Kresse and J. Furthmüller, Phys. Rev. B **54**, 11169 (1996).
[35] J. P. Perdew, J. A. Chevary, S. H. Vosko, K. A. Jackson, M. R. Pederson, D. J. Singh, and C. Fiolhais, Phys. Rev. B **46**, 6671 (1992).
[36] J. P. Perdew, K. Burke, and M. Ernzerhof, Phys. Rev. Lett. **77**, 3865 (1996).
[37] P. E. Blöchl, Phys. Rev. B **50**, 17953 (1994).
[38] G. Kresse and D. Joubert, Phys. Rev. B **59**, 1758 (1999).
[39] H. J. Monkhorst and J. D. Pack, Phys. Rev. B **13**, 5188 (1976).
[40] J. Neugebauer and M. Scheffler, Phys. Rev. B **46**, 16067 (1992).
[41] L. Bengtsson, Phys. Rev. B **59**, 12301 (1999).
[42] F. Edler, I. Miccoli, J. P. Stöckmann, H. Pfnür, C. Braun, S. Neufeld, S. Sanna, W. G. Schmidt, and C. Tegenkamp, Phys. Rev. B **95**, 125409 (2017).
[43] I. K. Robinson, P. A. Bennett, and F. J. Himpsel, Phys. Rev. Lett. **88**, 096104 (2002).
[44] D. Sánchez-Portal and R. M. Martin, Surf. Sci. **532–535**, 655 (2003).
[45] H. Ibach, H. D. Bruchmann, and H. Wagner, Appl. Phys. A **29**, 113 (1982).